GEOPHYSICS, VOL. 71, NO. 5 (SEPTEMBER-OCTOBER 2006); P. T151–T158, 7 FIGS.
10.1190/1.2335505

Modeling the scalar wave equation with Nyström methods

Jing-Bo Chen[1]

ABSTRACT

High-accuracy numerical schemes for modeling of the scalar wave equation based on Nyström methods are developed in this paper. Space is discretized by using the pseudospectral algorithm. For the time discretization, Nyström methods are used. A fourth-order symplectic Nyström method with pseudospectral spatial discretization is presented. This scheme is compared with a commonly used second-order scheme and a fourth-order nonsymplectic Nyström method. For a typical time-step size, the second-order scheme exhibits spatial dispersion errors for long-time simulations, while both fourth-order schemes do not suffer from these errors. Numerical comparisons show that the fourth-order symplectic algorithm is more accurate than the fourth-order nonsymplectic one. The capability of the symplectic Nyström method in approximately preserving the discrete energy for long-time simulations is also demonstrated.

INTRODUCTION

Seismic modeling is an important foundation of exploration seismology. High-accuracy seismic modeling schemes are increasing in demand as computing capacity increases. In this context, high-accuracy schemes are developed using Nyström time-stepping methods and pseudospectral spatial discretizations.

Numerical schemes for modeling of the scalar wave equation involve discretizations of both space and time. This discretizing process can be accomplished in two ways. The first way is to discretize both space and time simultaneously. The finite-difference methods (Claerbout, 1985) belong to this category. The second way is first to discretize space to obtain a system of ordinary differential equations (ODEs) with time as a variable and then to construct numerical schemes by discretizing time for the system of ODEs. The pseudospectral methods (Gazdag, 1981) and the finite-element methods (Ciarlet and Lions, 1991) fall into this second category.

To form a unified viewpoint and facilitate our understanding of numerical simulation schemes, we will accept that all numerical modeling schemes can be obtained by the second approach to discretization. Therefore, to construct modeling schemes for the scalar wave equation, we can first discretize space by finite-difference methods, pseudospectral methods, or finite-element methods. Second, we numerically integrate the resulting system of ordinary differential equations by discretizing time.

Note that the obtained system of ODEs is of second order. When numerically solving this system directly, we need to approximately evaluate additional starting values in addition to initial values. The higher the order of the schemes, the more complex the evaluation of the additional starting values.

Nyström methods are numerical methods designed for second-order differential equations. Nyström (1925) first considered this as a simplification of Runge-Kutta methods. Hairer et al. (1993) systematically developed Nyström methods. There are two benefits in using Nyström methods. First, we do not need to evaluate the additional starting values. Second, by introducing an intermediate variable, the scalar wave equation can be cast into a Hamiltonian system. Using Nyström methods, we can develop the corresponding symplectic methods. The symplectic methods have remarkable capability for long-time computations. This is because the symplectic properties guarantee that the numerical solution evolves in the same system as the solution of the original continuous differential equation (Feng, 1993; Sanz-Serna and Calvo, 1994).

In this paper, I present the pseudospectral method and explore high-order time discretizations. I follow this with a discussion of Nyström methods. I then develop a fourth-order symplectic Nyström method with pseudospectral spatial discretization. Finally, I illustrate the performance of this scheme with numerical experiments that compare it with a second-order scheme and a fourth-order nonsymplectic Nyström method.

PSEUDOSPECTRAL METHODS

As mentioned above, we can use finite-difference methods, pseudospectral methods, or finite-element methods for the space discretization. I use pseudospectral methods, for which the errors result

Manuscript received by the Editor July 18, 2005; revised manuscript received February 6, 2006; published online September 5, 2006.
[1]Chinese Academy of Sciences, Institute of Geology and Geophysics, P.O. Box 9825, Beijing 100029, China. E-mail: chenjb@mail.igcas.ac.cn.
© 2006 Society of Exploration Geophysicists. All rights reserved.

mainly from the time discretization. For higher accuracy, we need higher-order time discretization. The issue of computing additional starting values becomes more evident in this situation.

Pseudospectral methods for modeling of the scalar wave equation were presented by Gazdag (1981). The main point of the pseudospectral methods is to express the wavefield under consideration in terms of a complete set of orthogonal basis functions whose derivatives are known exactly. In practice, Fourier pseudospectral methods are usually employed.

Consider the scalar wave equation

$$\frac{\partial^2 u}{\partial t^2} = c^2\left(\frac{\partial^2 u}{\partial x^2} + \frac{\partial^2 u}{\partial y^2} + \frac{\partial^2 u}{\partial z^2}\right), \tag{1}$$

where $u(x,y,z,t)$ is the wavefield and $c(x,y,z)$ is the velocity. Let $\mathbf{u} = [u_{1,1,1}, \ldots, u_{N_x,N_y,N_z}]^T$, where T represents transpose and $u_{i,j,l}$ are the wavefield values at discrete locations, i.e., $u_{i,j,l} \approx u(i\Delta x, j\Delta y, l\Delta z, t)$; $i = 1, \ldots, N_x$; $j = 1, \ldots, N_y$; $l = 1, \ldots, N_z$. The values Δx, Δy, and Δz are grid increments in the x-, y-, and z-directions; and N_x, N_y, and N_z are the number of grid lines in the x-, y-, and z-directions, respectively. The semi-discrete system resulting from the pseudospectral method for equation 1 is

$$\frac{d^2\mathbf{u}}{dt^2} = c^2\mathcal{F}^{-1}[\mathbf{w} * \mathcal{F}(\mathbf{u})], \tag{2}$$

where $\mathcal{F}$ and $\mathcal{F}^{-1}$ represent 3D forward and inverse finite Fourier transforms, respectively, and $\mathbf{w} = [w_{1,1,1}, \ldots, w_{N_x,N_y,N_z}]^T$ with $w_{i,j,l} = -(k_{x_i}^2 + k_{y_j}^2 + k_{z_l}^2)$, where k_{x_i}, k_{y_j}, and k_{z_l} are discrete wavenumbers in the x-, y-, and z-directions, respectively. The asterisk $*$ denotes array multiplication between vectors. For example, suppose that $\mathbf{p} = (p_1, p_2, \ldots, p_m)$ and $\mathbf{q} = (q_1, q_2, \ldots, q_m)$, then $\mathbf{p} * \mathbf{q} = (p_1q_1, p_2q_2, \ldots, p_mq_m)$.

To obtain the final modeling scheme, we further discretize equation 2 in time. A standard second-order time difference is often used and gives

$$\begin{aligned}\mathbf{u}(t_0 + 2\Delta t) &= 2\mathbf{u}(t_0 + \Delta t) - \mathbf{u}(t_0)\\ &\quad + c^2\mathcal{F}^{-1}[\mathbf{w} * \mathcal{F}(\mathbf{u}(t_0 + \Delta t))]\Delta t^2,\end{aligned} \tag{3}$$

where Δt is the time-step size and t_0 is the initial time. As usual, we take $t_0 = 0$. To compute $\mathbf{u}(2\Delta t)$ using equation 3, we need to know $\mathbf{u}(0)$ and $\mathbf{u}(\Delta t)$, which can be computed from the initial conditions of equation 1: $u(0)$ and $\partial u(0)/\partial t$. We can evaluate $\mathbf{u}(0)$ directly from $u(0)$. To obtain $\mathbf{u}(\Delta t)$, a third-order scheme based on a Taylor series expansion was given by Gazdag (1981) as

$$u(\Delta t) = \sum_{i=0}^{3} \frac{\partial^i u(0)}{\partial t^i}\frac{(\Delta t)^i}{i!}. \tag{4}$$

In equation 4, $u(0)$ and $\partial u(0)/\partial t$ are known, $\partial^2 u(0)/\partial t^2$ is defined by equation 1, and $\partial^3 u(0)/\partial t^3$ is obtained by

$$\frac{\partial^3 u}{\partial t^3} = c^2\left(\frac{\partial^2}{\partial x^2} + \frac{\partial^2}{\partial y^2} + \frac{\partial^2}{\partial z^2}\right)\left(\frac{\partial u}{\partial t}\right),$$

which is obtained by substituting $\partial u/\partial t$ for u in equation 1. Finally, we can compute $\mathbf{u}(\Delta t)$ directly from $u(\Delta t)$.

The main error in scheme (equation) 3 is associated with the time differencing. Thus, to improve accuracy, we need to use a higher-order time difference. A natural choice is the fourth-order time difference

$$\begin{aligned}\boldsymbol{u}(4\Delta t) &= 16\mathbf{u}(3\Delta t) - 30\mathbf{u}(2\Delta t) + 16\mathbf{u}(\Delta t) - \mathbf{u}(0)\\ &\quad - 12c^2\mathcal{F}^{-1}[\mathbf{w} * \mathcal{F}(\mathbf{u}(2\Delta t))]\Delta t^2.\end{aligned} \tag{5}$$

However, we can show that scheme 5 is unconditionally unstable by using the standard spectral analysis. Using the Taylor series and the wave equation, another approach for high-order time differencing was presented by Etgen (1986). But this approach still requires the computation of additional starting values. For example, for a fourth-order method, we need a fifth-order scheme to compute the starting values instead of the third-order scheme 4. We are faced with a cumbersome procedure for computing starting values. Therefore, an alternative approach is needed.

NYSTRÖM METHODS

The basic idea of Nyström (1925) methods is as follows: First introduce an intermediate variable to reduce the second-order wave equation to an equivalent first-order system; then apply Runge-Kutta methods to the first-order system and simplify by taking advantage of the special form of the first-order system. The obtained Nyström methods do not need to evaluate starting values and have considerably less computational cost than Runge-Kutta methods applied directly to the first-order system for second-order equations such as equation 2. For details, refer to Hairer et al. (1993).

For our purposes, consider a second-order system of ordinary differential equations written in the form

$$\frac{d^2\mathbf{y}}{dt^2} = \mathbf{f}(\mathbf{y}). \tag{6}$$

A Nyström method for system 6 reads

$$\begin{aligned}\mathbf{Z}_i &= \mathbf{f}\left(\mathbf{y}_0 + c_i\Delta t\mathbf{z}_0 + \Delta t^2\sum_{j=1}^{s} a_{ij}\mathbf{Z}_j\right), \quad i = 1, 2, \ldots, s,\\ \mathbf{y}_1 &= \mathbf{y}_0 + \Delta t\mathbf{z}_0 + \Delta t^2\sum_{i=1}^{s} \bar{b}_i\mathbf{Z}_i,\\ \mathbf{z}_1 &= \mathbf{z}_0 + \Delta t\sum_{i=1}^{s} b_i\mathbf{Z}_i,\end{aligned} \tag{7}$$

where $\mathbf{z} = d\mathbf{y}/dt$, $\mathbf{y}_0 = \mathbf{y}(0)$, $\mathbf{z}_0 = \mathbf{z}(0)$, $\mathbf{y}_1 \approx \mathbf{y}(\Delta t)$, $\mathbf{z}_1 \approx \mathbf{z}(\Delta t)$ and where c_i, a_{ij}, $\bar{b}_i$, and b_i are constants that determine the order of the method. The numerical solution $\mathbf{y}_1$ is obtained through auxiliary variables $\mathbf{Z}_i$ in scheme 7.

The starting values $\mathbf{y}_0$ and $\mathbf{z}_0 = d\mathbf{y}(0)/dt$ in scheme 7 are both known, and no additional starting values are needed. Scheme 7 requires computation of $\mathbf{z}_1$, but this is easy to accomplish because the main evaluations of $\mathbf{Z}_i$ have been done previously in the computation of $\mathbf{y}_1$.

The order conditions (via the algebraic equations satisfied by c_i, a_{ij}, $\bar{b}_i$, and b_i) have been obtained by using tree theory in Hairer et al. (1993). By solving these algebraic equations, we can obtain the corresponding methods. Consider a stable fourth-order explicit method (Qin and Zhu, 1991):

$$c_1 = \frac{3+\sqrt{3}}{6}, \quad c_2 = \frac{3-\sqrt{3}}{6}, \quad c_3 = \frac{3+\sqrt{3}}{6},$$

$$\bar{b}_1 = \frac{5-3\sqrt{3}}{24}, \quad \bar{b}_2 = \frac{3+\sqrt{3}}{12}, \quad \bar{b}_3 = \frac{1+\sqrt{3}}{24},$$

$$b_1 = \frac{3-2\sqrt{3}}{12}, \quad b_2 = \frac{1}{2}, \quad b_3 = \frac{3+2\sqrt{3}}{12},$$

$$a_{21} = \frac{2-\sqrt{3}}{12}, \quad a_{32} = \frac{\sqrt{3}}{6},$$

$$a_{11} = a_{12} = a_{13} = a_{22} = a_{23} = a_{31} = a_{33} = 0.$$

With these coefficients, scheme 7 becomes

$$\mathbf{Z}_1 = \mathbf{f}\left(\mathbf{y}_0 + \frac{3+\sqrt{3}}{6}\Delta t\mathbf{z}_0\right),$$

$$\mathbf{Z}_2 = \mathbf{f}\left(\mathbf{y}_0 + \frac{3-\sqrt{3}}{6}\Delta t\mathbf{z}_0 + \frac{2-\sqrt{3}}{12}\Delta t^2\mathbf{Z}_1\right),$$

$$\mathbf{Z}_3 = \mathbf{f}\left(\mathbf{y}_0 + \frac{3+\sqrt{3}}{6}\Delta t\mathbf{z}_0 + \frac{\sqrt{3}}{6}\Delta t^2\mathbf{Z}_2\right),$$

$$\mathbf{y}_1 = \mathbf{y}_0 + \Delta t\mathbf{z}_0 + \Delta t^2\left(\frac{5-3\sqrt{3}}{24}\mathbf{Z}_1 + \frac{3+\sqrt{3}}{12}\mathbf{Z}_2 + \frac{1+\sqrt{3}}{24}\mathbf{Z}_3\right),$$

$$\mathbf{z}_1 = \mathbf{z}_0 + \Delta t\left(\frac{3-2\sqrt{3}}{12}\mathbf{Z}_1 + \frac{1}{2}\mathbf{Z}_2 + \frac{3+2\sqrt{3}}{12}\mathbf{Z}_3\right). \tag{8}$$

Another benefit of Nyström methods is that we can develop symplectic algorithms if equation 6 possesses a symplectic structure. In the past, we only focused on the accuracy of the numerical methods when solving differential equations numerically. However, with the tremendous progress in computer technology and numerical analysis theory in recent decades, computation has become a third category of methods in scientific research in addition to theory and experiment. Not only is the accuracy of numerical methods expected, but structure-preserving properties also are required. Solutions to differential equations usually preserve various structures such as symplectic structure, multisymplectic structure, and various geometric structures. When solving differential equations numerically, some numerical methods also preserve these structures (they are usually called structure-preserving algorithms), while others violate them. The structure-preserving methods have remarkable capability for long-time computation. The scalar wave equation 1 has a classical Hamiltonian structure (Chen, 2004). Therefore, we can develop the corresponding structure-preserving methods (see Appendix A).

A PSEUDOSPECTRAL METHOD WITH FOURTH-ORDER NYSTRÖM TIME DIFFERENCE

Now we return to the issue of higher-order time difference for equation 2. Equation 2 is a second-order system of ordinary differential equations obtained from equation 1 by using pseudospectral methods. Therefore, Nyström methods can be applied directly. We introduce a variable $\mathbf{v} = d\mathbf{u}/dt$ and apply Nyström method 8 to equation 2 to obtain

$$\mathbf{V}_1 = c^2\mathcal{F}^{-1}\left[\mathbf{w} * \mathcal{F}\left(\mathbf{u}_0 + \frac{3+\sqrt{3}}{6}\Delta t\mathbf{v}_0\right)\right],$$

$$\mathbf{V}_2 = c^2\mathcal{F}^{-1}\left[\mathbf{w} * \mathcal{F}\left(\mathbf{u}_0 + \frac{3-\sqrt{3}}{6}\Delta t\mathbf{v}_0 + \frac{2-\sqrt{3}}{12}\Delta t^2\mathbf{V}_1\right)\right],$$

$$\mathbf{V}_3 = c^2\mathcal{F}^{-1}\left[\mathbf{w} * \mathcal{F}\left(\mathbf{u}_0 + \frac{3+\sqrt{3}}{6}\Delta t\mathbf{v}_0 + \frac{\sqrt{3}}{6}\Delta t^2\mathbf{V}_2\right)\right],$$

$$\mathbf{u}_1 = \mathbf{u}_0 + \Delta t\mathbf{v}_0 + \Delta t^2\left(\frac{5-3\sqrt{3}}{24}\mathbf{V}_1 + \frac{3+\sqrt{3}}{12}\mathbf{V}_2 + \frac{1+\sqrt{3}}{24}\mathbf{V}_3\right),$$

$$\mathbf{v}_1 = \mathbf{v}_0 + \Delta t\left(\frac{3-2\sqrt{3}}{12}\mathbf{V}_1 + \frac{1}{2}\mathbf{V}_2 + \frac{3+2\sqrt{3}}{12}\mathbf{V}_3\right). \tag{9}$$

Scheme 9 is a stable fourth-order explicit Nyström method with accuracy of $\mathcal{O}(\Delta t^4)$ (Qin and Zhu, 1991; Hairer et al., 1993). Because we use pseudospectral spatial discretization, the spatial accuracy is of exponential order $\mathcal{O}(\exp(\Delta x))$ (Fornberg, 1996). Therefore, the total accuracy of scheme 9 is $\mathcal{O}(\Delta t^4 + \exp(\Delta x))$. As pointed out by Hairer et al. (1993), the Nyström method (scheme 9) is considerably more efficient than Runge-Kutta methods.

In seismic modeling based on scheme 9, we compute $\mathbf{u}_1$ and $\mathbf{v}_1$ from known $\mathbf{u}_0$ and $\mathbf{v}_0 = d\mathbf{u}_0/dt$. Then we repeat this process with $\mathbf{u}_0$ and $\mathbf{v}_0$ replaced by $\mathbf{u}_1$ and $\mathbf{v}_1$, respectively. Higher-order Nyström time differences are easily available, and they have the same format as scheme 9 but with more $\mathbf{V}_i$s.

NUMERICAL EXPERIMENTS

In this section, we perform numerical experiments to test the feasibility and performance of the presented scheme. For clarity and simplicity, we only consider the 2D case. As in Gazdag (1981), we use the initial conditions

$$u(x,z,t=0) = \exp[-0.0001(x^2 + (z-z_0)^2)]$$

and

$$\frac{\partial u(0)}{\partial t} = 0.$$

The grid increments are $\Delta x = \Delta z = 50$ m. Here, z_0 is a constant that indicates the position of the source. In the following numerical examples, we use periodic boundary conditions.

In the first example, we use scheme 9 to simulate wave propagation in a heterogeneous medium. The velocity model (Figure 1) consists of three layers with velocities $c = 1000$ m/s, 2000 m/s, and 3000 m/s; a straight interface; and a curved interface. The source is set at ($x = 0$ m, $z = 200$ m). The time-step size Δt is 0.006 s. Figure 2 shows the wavefield at $t = 0$, 0.438, 0.936, 1.248, 1.56, and 1.872 s. The simulated reflection and transmission phenomena are qualitatively correct.

We now make numerical comparisons between scheme 9 and the commonly used scheme 3. In this example, we use the velocity c = 3000 m/s and the time step size Δt = 0.006 s. The starting value for equation 3 is computed through equation 4, which requires evaluating the second-order spatial derivatives of the initial conditions. Therefore, when using schemes like equation 3 in wave simulation, we usually require that the initial conditions have a certain degree of smoothness, which sometimes is not satisfied in practice (for example, discrete initial conditions). In contrast, when using scheme 9, we have no special requirement on the initial conditions, which makes schemes like 9 more practical. In Figure 3, we show the impulse responses for schemes 3 and 9 after 200, 500, and 5000 time steps, respectively. For time steps equal to or less than 200, impulse responses for both schemes 3 and 9 do not exhibit spatial dispersion errors. After 500 time steps, the spatial dispersion becomes evident in the wavefront computed with scheme 3, which contrasts with the clean wavefront computed with scheme 9 (Figure 3c and d). After 5000 time steps (t = 30 s), the wavefront computed with scheme 3 has blurred very badly, but the wavefront computed with scheme 9 is still sharp (Figure 3e and f). These observations indicate that for a typical time-step size of 0.006 s, the commonly used scheme 3 is not suitable for lengthy simulations.

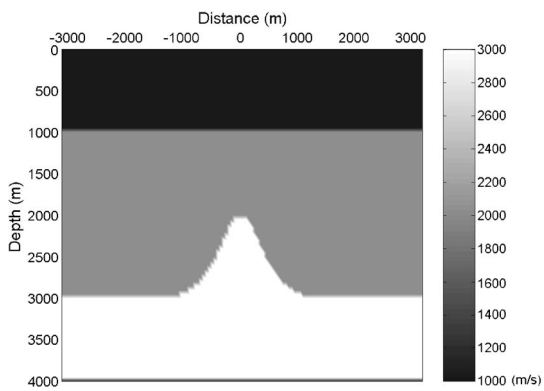

Figure 1. The velocity model used for the numerical experiments. It consists of three layers with velocities c = 1000 m/s, 2000 m/s, and 3000 m/s, respectively; a straight interface; and a curved interface.

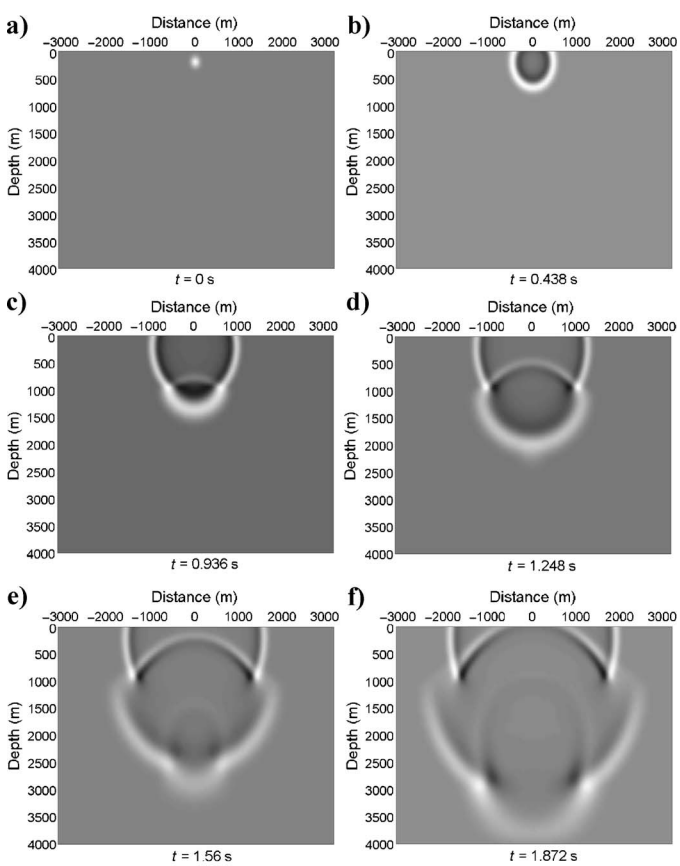

Figure 2. Wavefield evolution with time computed with scheme 9. Distance and time are measured in meters and seconds, respectively.

Now we perform simulations by scheme 3 with smaller time-step sizes of 0.004, 0.003, 0.002, and 0.001 s. To compute the wavefront at 30 s, the number of time steps is 7500, 10,000, 15,000, and 30,000, respectively. Figure 4 shows the simulation results. We see that dispersion errors decrease as time-step size decreases. The result with time-step size of 0.001 s is similar to that obtained with scheme 9 with a time-step size of 0.006 s (Figure 3d). This indicates that to obtain the impulse response at 30 s, scheme 9 with a time-step size of 0.006 s is more efficient than scheme 3 with a time-step size of 0.001 s.

We can explain this as follows: Although for each time step scheme 9 needs to compute three pairs of FFTs (forward and inverse), which is three times as many as that of the scheme 3, the time-step size used in scheme 9 is six times as large as that used in scheme 3. Because the main computational cost in both schemes 9 and 3 is the computation of FFTs, the overall computational cost of scheme 9 is only half that of scheme 3.

To demonstrate the advantages of the symplectic method, we now make numerical comparisons between the fourth-order symplectic Nyström scheme 9 with the following fourth-order nonsymplectic Nyström scheme:

$$\begin{aligned}
\mathbf{V}_1 &= c^2\mathcal{F}^{-1}[\mathbf{w} * \mathcal{F}(\mathbf{u}_0)],\\
\mathbf{V}_2 &= c^2\mathcal{F}^{-1}\left[\mathbf{w} * \mathcal{F}\left(\mathbf{u}_0 + \frac{1}{2}\Delta t\mathbf{v}_0 + \frac{1}{8}\Delta t^2\mathbf{V}_1\right)\right],\\
\mathbf{V}_3 &= c^2\mathcal{F}^{-1}\left[\mathbf{w} * \mathcal{F}\left(\mathbf{u}_0 + \Delta t\mathbf{v}_0 + \frac{1}{2}\Delta t^2\mathbf{V}_2\right)\right],\\
\mathbf{u}_1 &= \mathbf{u}_0 + \Delta t\mathbf{v}_0 + \Delta t^2\left(\frac{1}{6}\mathbf{V}_1 + \frac{1}{3}\mathbf{V}_2\right),\\
\mathbf{v}_1 &= \mathbf{v}_0 + \Delta t\left(\frac{1}{6}\mathbf{V}_1 + \frac{2}{3}\mathbf{V}_2 + \frac{1}{6}\mathbf{V}_3\right).
\end{aligned} \tag{10}$$

Figure 5 shows the impulse response computed with scheme 10 after 5000 time steps. The time-step size is 0.006 s. We see that the result is similar to that computed with the symplectic scheme 9 (Figure 3f). To examine more closely the results obtained by these two fourth-order schemes, amplitude curves at a fixed point (x = −1600 m, z = 1600 m) over the time near 30 s (5000 time steps) are shown in Figure 6a. We see discrepancy in the amplitude curves computed by the two fourth-order schemes. In Figure 6b, another amplitude curve is added, which is computed by the nonsymplectic scheme 10 with a smaller time step size of 0.001 s. It can be seen that the amplitude curve computed by the symplectic scheme 9 with a time-step size of 0.006 s agrees well with the amplitude curve com-

puted by the nonsymplectic scheme 10 with a smaller time-step size of 0.001 s. This indicates that the fourth-order symplectic algorithm scheme 9 is more accurate than the fourth-order nonsymplectic algorithm scheme 10 for the same time-step size. To show how the amplitude curves computed by the nonsymplectic scheme 10 with smaller time-step sizes approach the amplitude curve computed by the symplectic scheme 9 with a time-step size of 0.006 s, we plot the following amplitude-difference curves (Figure 6c):

$$AD_{\Delta t}(t) = S_{0.006}(t) - NS_{\Delta t}(t),$$

where $AD_{\Delta t}(t)$ denotes the amplitude-difference curve; $S_{0.006}(t)$, the amplitude curve computed by the symplectic scheme 9 with a time-step size of 0.006 s; and $NS_{\Delta t}(t)$, the amplitude curve computed by the nonsymplectic scheme 10 with a time-step size of Δt. Here we take $\Delta t = 0.006, 0.004, 0.002$, and 0.001 s. We can see that the magnitude of the curves of the amplitude difference diminishes with decreasing Δt.

From the above numerical comparisons, we can conclude that to achieve approximately the same accuracy, the symplectic algorithm scheme 9 is much more efficient than the nonsymplectic algorithm scheme 10, considering the time-step sizes used. This is a great advantage.

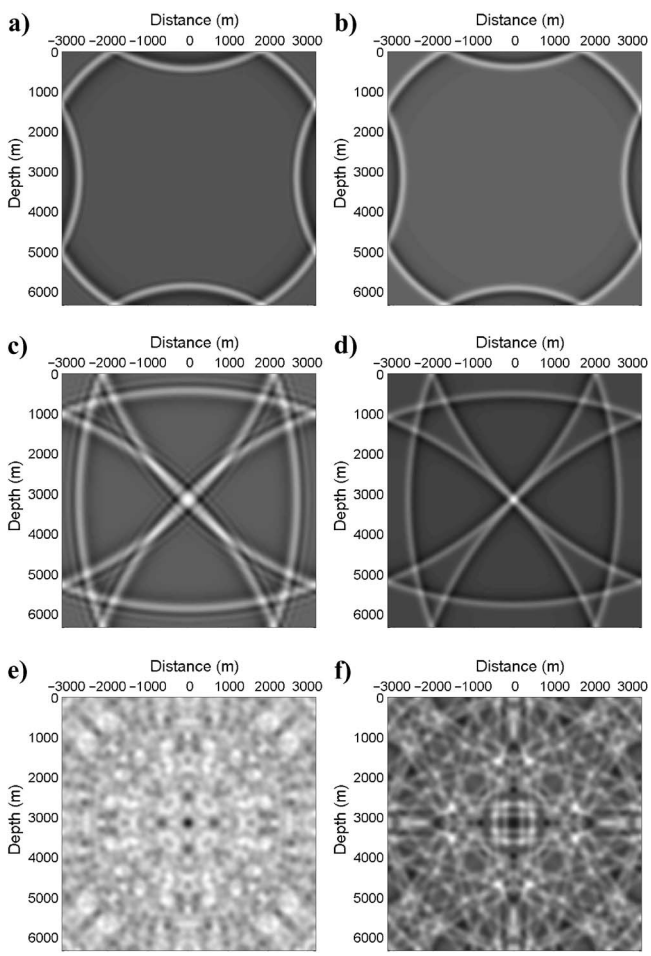

Figure 3. Impulse responses computed with schemes 3 and 9. (a) and (b) 200 time steps; (c) and (d) 500 time steps; (e) and (f) 5000 time steps. Views (a), (c), and (e) are computed with scheme 3; (b), (d), and (f) are computed with scheme 9.

Another important advantage of a symplectic algorithm is its ability to approximately preserve energy for lengthy simulations (Feng, 1993; Sanz-Serna and Calvo, 1994). For the wave equation $u_{tt} = c^2(u_{xx} + u_{zz})$ with a periodic boundary condition, the true solution preserves the energy

$$\int_{\mathcal{M}} (v^2 + c^2(u_x^2 + u_z^2))dxdz,$$

where $v = u_t$ and $\mathcal{M}$ is the integral domain.

Now in our numerical experiments, we monitor the discrete energy

$$G(n) = \sum_{i,l} \left[(v_{i,l}^n)^2 + c^2\left(\frac{u_{i+1,l}^n - u_{i,l}^n}{\Delta x}\right)^2 + c^2\left(\frac{u_{i,l+1}^n - u_{i,l}^n}{\Delta z}\right)^2 \right] \Delta x \Delta z,$$

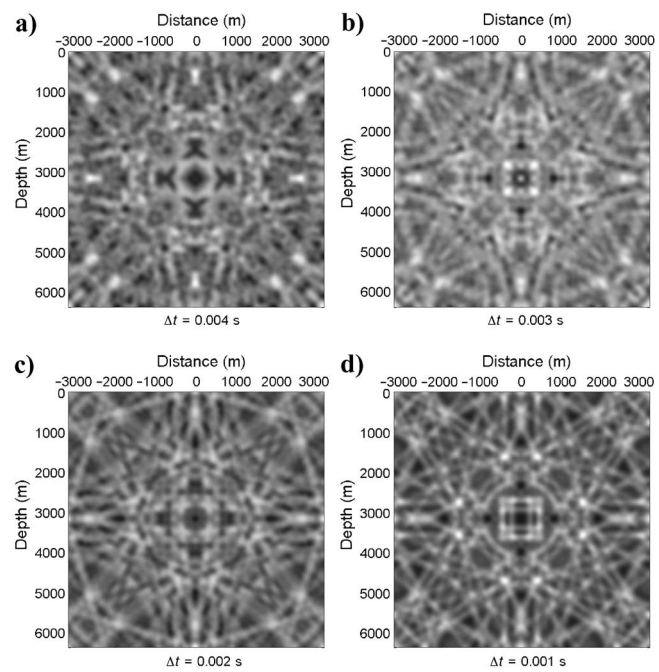

Figure 4. Impulse response at 30 s. The results are computed with scheme 3 with time-step sizes of 0.004, 0.003, 0.002, and 0.001 s, respectively.

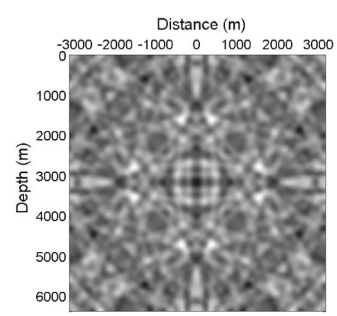

Figure 5. Impulse response after 5000 time steps computed with scheme 10 with a step-time size of 0.006 s.

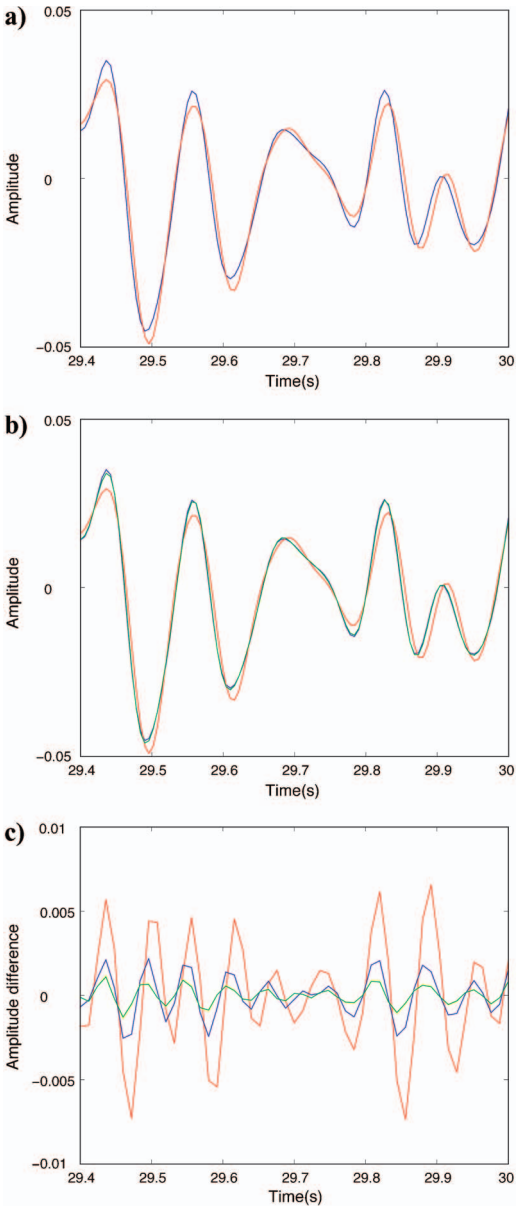

Figure 6. Amplitude and amplitude-difference curves at a fixed point ($x = -1600$ m, $z = 1600$ m) over the time near 30 s. (a) Amplitude curves computed by the symplectic scheme 9 with $\Delta t = 0.006$ s (blue line) and the nonsymplectic scheme 10 with $\Delta t = 0.006$ s (red line). (b) Amplitude curves computed by the symplectic scheme 9 with $\Delta t = 0.006$ s (blue line); the nonsymplectic scheme 10 with $\Delta t = 0.006$ s (red line); and the nonsymplectic scheme 10 with $\Delta t = 0.001$ s (green line). (c) Amplitude-difference curves: $\Delta t = 0.006$ s (red line); $\Delta t = 0.004$ s (blue line); $\Delta t = 0.002$ s (yellow line); and $\Delta t = 0.001$ s (green line).

where $v_{i,l}^n \approx v(i\Delta x, l\Delta z, n\Delta t)$, $u_{i,l}^n \approx u(i\Delta x, l\Delta z, n\Delta t)$, and $n = 0, 1, 2, \ldots, N$. Here, N is the number of time steps.

Figure 7a shows the discrete energy curves [$G(n)$ as a function n] for both schemes 9 and 10, with $N = 5000$. For the symplectic scheme 9, the energy curve fluctuates about a constant energy. For the nonsymplectic scheme 10, a numerical loss in energy is observed. The corresponding result for $N = 100{,}000$ is shown in Figure 7b. For this very long computation, the energy curve for the symplectic scheme 9 still fluctuates about a constant energy while nearly half of the energy is lost in the energy curve for the nonsymplectic scheme 10. This demonstrates the capability of the symplectic algorithm for approximately preserving the discrete energy for lengthy computations.

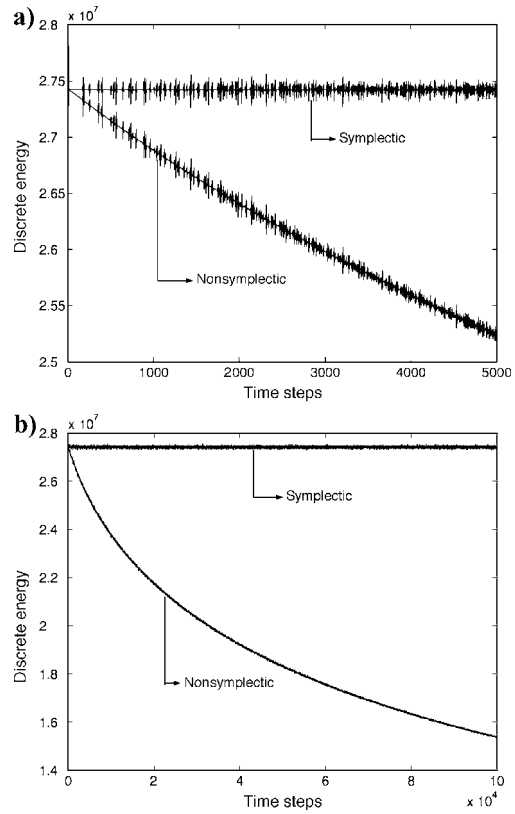

Figure 7. Discrete energy curves [$G(n)$ versus n] for the symplectic scheme 9 and the nonsymplectic scheme 10. (a) N = 5000; (b) N = 100,000.

CONCLUSIONS

Nyström time differencing with pseudospectral spatial discretizaiton is presented for modeling of the scalar wave equation. Two fourth-order Nyström schemes with pseudospectral spatial discretizaiton are developed; one is symplectic and the other is nonsymplectic. Numerical experiments demonstrate three results. First, these fourth-order schemes can be used for long-time simulations with a time-step size of 0.006 s, whereas the commonly used second-order scheme exhibits severe dispersion errors for this computation time and time-step size. Second, the fourth-order schemes with a time-step size of 0.006 s are more efficient than the second-order scheme with a small time-step size of 0.001 s. And third, the symplectic algorithm is more accurate than the nonsymplectic algorithm and has a better capability of approximately preserving the discrete energy for lengthy simulations.

Preserving propagation energy is only one feature of preserving symplectic structure. The symplectic algorithms also have other features such as better accuracy, which can be explained by the theory of backward error analysis (Hairer et al., 2002). According to this theory, the solutions of both symplectic and nonsymplectic algorithms for a Hamiltonian system formally satisfy a perturbed system.

However, the perturbed system satisfied by the symplectic algorithms retains the Hamiltonian structure; the system satisfied by the nonsymplectic algorithms does not.

ACKNOWLEDGMENTS

I would like to thank professor Arcone and anonymous reviewers for valuable suggestions and corrections, that led to a great improvement of this paper. This work is supported by the National Natural Science Foundation of China under grant 40474047 and also partially by the Chinese Academy of Sciences with Key Project of Knowledge Innovation KZCX1-SW-18.

APPENDIX A

HAMILTONIAN STRUCTURE

In this appendix, I present the Hamiltonian structure and the corresponding symplectic algorithms for the scalar wave equation. Introducing an intermediate variable $v = du/dt$, equation 1 is equivalent to

$$\frac{\partial u}{\partial t} = v,$$
$$\frac{\partial v}{\partial t} = c^2\left(\frac{\partial^2 u}{\partial x^2} + \frac{\partial^2 u}{\partial y^2} + \frac{\partial^2 u}{\partial z^2}\right). \tag{A-1}$$

Equation A-1 can be reformulated as

$$\frac{\partial}{\partial t}\begin{bmatrix} u \\ v \end{bmatrix} = \begin{bmatrix} 0 & 1 \\ -1 & 0 \end{bmatrix}\begin{bmatrix} \dfrac{\delta \mathcal{H}}{\delta u} \\ \dfrac{\delta \mathcal{H}}{\delta v} \end{bmatrix}, \tag{A-2}$$

where

$$\mathcal{H} = \frac{1}{2}\int\left[v^2 + c^2\left(\left(\frac{\partial u}{\partial x}\right)^2 + \left(\frac{\partial u}{\partial y}\right)^2 + \left(\frac{\partial u}{\partial z}\right)^2\right)\right]dxdy$$

is the Hamiltonian system, and δ denotes the variational derivative.

Equation A-2 is an infinite-dimensional Hamiltonian system. The evolution of the wavefield with time is characterized by a symplectic structure $\int du \wedge dv dxdy$, which can be viewed as an antisymmetric quadratic form. For the exact definition of symplectic structure, as well as the infinite-dimensional Hamiltonian system and variational derivative, see Olver (1993).

In solving equation A-2 numerically, we can use finite-difference, finite-element, or pseudospectral methods to discretize the space and obtain a finite-dimensional system. Equation 2, which is obtained with a pseudospectral method, can be cast into a finite-dimensional Hamiltonian system. First, introducing $\mathbf{v} = d\mathbf{u}/dt$, we can rewrite equation A-2 as

$$\frac{d\mathbf{u}}{dt} = \mathbf{v},$$
$$\frac{d\mathbf{v}}{dt} = c^2\mathcal{F}^{-1}[\mathbf{w} * \mathcal{F}(\mathbf{u})]. \tag{A-3}$$

Further, we can reformulate equation A-3 as

$$\frac{d}{dt}\begin{bmatrix} \mathbf{u} \\ \mathbf{v} \end{bmatrix} = \begin{bmatrix} 0 & I \\ -I & 0 \end{bmatrix}\begin{bmatrix} \dfrac{\partial H}{\partial \mathbf{u}} \\ \dfrac{\partial H}{\partial \mathbf{v}} \end{bmatrix}, \tag{A-4}$$

where I is an identity matrix and $H = \frac{1}{2}[\mathbf{v}^T\boldsymbol{v} + c^2\mathbf{u}^T D\mathbf{u}]$. The matrix D is a second-order spectral differential matrix which satisfies

$$\mathcal{F}^{-1}[\mathbf{w} * \mathcal{F}(\mathbf{u})] = D\mathbf{u}.$$

For details about spectral differential matrix, see Chen and Qin (2001). Equation A-4 is a standard finite-dimensional Hamiltonian system. A finite-dimensional Hamiltonian system is just a system of ordinary differential equations that has the form of equation A-4. The true solution of equation A-4 preserves the symplectic structure $d\mathbf{u} \wedge d\mathbf{v}$. In other words, if we suppose that the solution of equation A-4 is $P = F(P_0)$, where $P = [\boldsymbol{u}, \mathbf{v}]^T$ and $P_0 = [\mathbf{u}(t = 0), \mathbf{v}(t = 0)]^T$, then the fact that $F(P_0)$ preserves the symplectic structure $d\mathbf{u} \wedge d\mathbf{v}$ is equivalent to $F(P_0)$ satisfying

$$\left[\frac{\partial F}{\partial P_0}\right]J\left[\frac{\partial F}{\partial P_0}\right]^T = J, \quad \text{where } J = \begin{bmatrix} 0 & I \\ -I & 0 \end{bmatrix}.$$

Here, $[\partial F/\partial P_0]$ is the Jacobian of the vector-valued function $F(P_0)$. A function satisfying the above equality is also called a symplectic mapping. Thus, it is concluded that the time evolution of the seismic wavefield is a symplectic mapping. In seismic modeling, we need to solve equation A-4 numerically. Suppose that $\widetilde{F}(P_0)$ is the numerical solution of equation A-4 obtained by some numerical algorithm. Of course, the numerical solution $\widetilde{F}(P_0)$ is the approximation of the true solution $F(P_0)$. Does the numerical solution also have other properties? In fact, some numerical solutions are symplectic mappings while others are not. A numerical method is called a symplectic algorithm if the resulting numerical solution is a symplectic mapping. In the past, we mainly focused on the accuracy of the numerical solution to a Hamiltonian system; its structure-preserving properties were not considered seriously. With the introduction of symplectic algorithms and its great success in many physical fields, structure-preserving algorithms have developed into a very active and promising research area. The Hamiltonian framework developed here provides a basis for applying symplectic algorithms in seismic modeling. Based on this framework, we should develop numerical solutions of equation A-4 that are also symplectic mappings, i.e., symplectic algorithms. Various symplectic algorithms for Hamiltonian systems have been developed. We can directly apply the symplectic algorithms to equation A-4. Based on a finite-difference spatial discretization, Hamiltonian systems also can be obtained (Luo

et al., 2001). However, this kind of spatial discretization usually causes spatial dispersion errors.

Now consider a Nyström formulation for equation A-4:

$$\mathbf{V}_i = c^2\mathcal{F}^{-1}\left[\mathbf{w} * \mathcal{F}\left(\mathbf{u}_0 + c_i\Delta t\mathbf{z}_0 + \Delta t^2\sum_{j=1}^{s} a_{ij}\mathbf{V}_j\right)\right],$$

$$\mathbf{u}_1 = \mathbf{u}_0 + \Delta t\mathbf{v}_0 + \Delta t^2\sum_{i=1}^{s}\bar{b}_i\mathbf{V}_i, \quad \mathbf{v}_1 = \mathbf{v}_0 + \Delta t\sum_{i=1}^{s} b_i\mathbf{V}_i. \tag{A-5}$$

If the coefficients in scheme A-5 satisfy

$$\bar{b}_i = b_i(1 - c_i), \quad i = 1, \ldots, s,$$

$$b_i(\bar{b}_j - a_{ij}) = b_j(\bar{b}_i - a_{ji}), \quad i,j = 1, \ldots, s,$$

then scheme A-5 is a symplectic algorithm (Sanz-Serna and Calvo, 1994). It is easy to check that the coefficients used in scheme 9 satisfy the above conditions; therefore, scheme 9 is a symplectic algorithm.

REFERENCES

Chen, J. B., 2004, Multisymplectic geometry for the seismic wave equation: Communications in Theoretical Physics, **41**, 561–566.

Chen, J. B., and M. Z. Qin, 2001, Multisymplectic Fourier pseudospectral method for the nonlinear Schrödinger equation: Electronic Transactions on Numerical Analysis, **12**, 193–204.

Ciarlet, P. G., and J. L. Lions, 1991, Handbook of numerical analysis: North-Holland.

Claerbout, J. F., 1985, Imaging the earth's interior: Blackwell Scientific Publications, Inc.

Etgen, J. T., 1986, High-order finite-difference reverse migration with the two-way non-reflecting wave equation: SEP-48: Stanford University.

Feng, K., 1993, The collected works of Feng Kang: Defence Industrial Press.

Fornberg, B., 1996, A practical guide to pseudospectral method: Cambridge Univ. Press.

Gazdag, J., 1981, Modeling of the acoustic wave equation with transform methods: Geophysics, **46**, 854–859.

Hairer, E., C. Lubich, and G. Warnner, 2002, Geometric numerical integration: Springer-Verlag, Berlin.

Hairer, E., S. P. Nøsett, and G. Warnner, 1993, Solving ordinary differential equations I: Springer-Verlag, Berlin.

Luo, M. Q., H. Liu, and Y. M. Li, 2001, Hamiltonian description and symplectic method of seismic wave propagation: Chinese Journal of Geophysics, 44, 120–128.

Nyström, E. J., 1925, Über die numerische integration von differentialgleichungen: Acta Societe Scientiarum Fennicae, 50, 1–54.

Olver, P. J., 1993, Applications of Lie groups to differential equations: Springer-Verlag, New York.

Qin, M. Z., and W. J. Zhu, 1991, Canonical Runge-Kutta-Nyström methods for second order ODE's: Computational Mathematics Applications, **22**, 85–95.

Sanz-Serna, J. M., and M. Calvo, 1994, Numerical Hamiltonian problems: Chapman and Hall.